Geothermics 88 (2020) 101865

Contents lists available at ScienceDirect

Geothermics

journal homepage: www.elsevier.com/locate/geothermics

Increased Power Generation due to Exothermic Water Exsolution in CO_2 Plume Geothermal (CPG) Power Plants

Mark R. Fleming[a,*], Benjamin M. Adams[b], Thomas H. Kuehn[a], Jeffrey M. Bielicki[c,d], Martin O. Saar[b,e,**]

[a] Department of Mechanical Engineering, University of Minnesota, 111 Church St SE, Minneapolis, MN 55455, USA
[b] Geothermal Energy and Geofluids Group, Department of Earth Sciences, ETH-Zürich, Sonneggstr. 5, 8092 Zürich, Switzerland
[c] Department of Civil, Environmental, and Geodetic Engineering, 2070 Neil Avenue, Columbus, OH 43210, USA
[d] John Glenn College of Public Affairs, 1810 College Road, Columbus, OH 43210, USA
[e] Department of Earth and Environmental Sciences, University of Minnesota, 116 Church St SE, Minneapolis, MN 55455, USA

ARTICLE INFO

Keywords:
Carbon Dioxide Plume Geothermal
Carbon Dioxide Vertical Well
H_2O-CO_2 Solubility
Exothermic H_2O Exsolution

ABSTRACT

A direct CO_2-Plume Geothermal (CPG) system is a novel technology that uses captured and geologically stored CO_2 as the subsurface working fluid in sedimentary basin reservoirs to extract geothermal energy. In such a CPG system, the CO_2 that enters the production well is likely saturated with H_2O from the geothermal reservoir. However, direct CPG models thus far have only considered energy production via pure (i.e. dry) CO_2 in the production well and its direct conversion in power generation equipment. Therefore, we analyze here, how the wellhead fluid pressure, temperature, liquid water fraction, and the resultant CPG turbine power output are impacted by the production of CO_2 saturated with H_2O for reservoir depths ranging from 2.5 km to 5.0 km and geothermal temperature gradients between 20 °C/km and 50 °C/km. We demonstrate that the H_2O in solution is exothermically exsolved in the vertical well, increasing the fluid temperature relative to dry CO_2, resulting in the production of liquid H_2O at the wellhead. The increased wellhead fluid temperature increases the turbine power output on average by 15% to 25% and up to a maximum of 41%, when the water enthalpy of exsolution is considered and the water is (conservatively) removed before the turbine, which decreases the fluid mass flow rate through the turbine and thus power output. We show that the enthalpy of exsolution and the CO_2-H_2O solution density are fundamental components in the calculation of CPG power generation and thus should not be neglected or substituted with the properties of dry CO_2.

1. Introduction

The emission of carbon dioxide (CO_2) to, and its accumulation in, the atmosphere is a strong driver of climate change and the associated increase in the global mean surface temperature of Earth. For example, the Intergovernmental Panel on Climate Change (IPCC) has unequivocally concluded that the generation of electricity and heat by the combustion of fossil fuels is responsible for at least 25% of the total amount of CO_2 that has been emitted by human activities (IPCC, 2014). Renewable energy sources, such as wind, solar, bio-energy, and geothermal energy, have been developed and used to generate power with few, if any, operational CO_2 emissions, thereby reducing the overall emission of CO_2 for electricity generation. However, of these renewable energy sources only geothermal and bio-energy systems can provide continuous baseload power (Matek and Gawell, 2015). To further reduce CO_2 emissions into the atmosphere, existing power plants can be retrofitted to capture CO_2 and store the captured CO_2 underground in geologic formations in what is typically termed a carbon or CO_2 capture and (geologic) storage (CCS) process (IPCC, 2005; Michael et al., 2010; Piri et al., 2005). This process can isolate CO_2 underground in saline reservoirs or (partially) depleted oil or gas reservoirs, which are overlain by a low- to almost zero-permeability caprock, such that the leakage risk of the buoyant CO_2 is minimal (Bielicki et al., 2016, 2015, 2014; IPCC, 2005).

The geologically stored CO_2 can be used as a heat extraction fluid for geothermal systems, which is considered to be a CO_2 capture,

* Corresponding author.
** Corresponding author at: Geothermal Energy and Geofluids Group, Department of Earth Sciences, ETH-Zürich, Sonneggstr. 5, 8092 Zürich, Switzerland.
E-mail addresses: flemi311@umn.edu (M.R. Fleming), badams@ethz.ch (B.M. Adams), kuehn001@umn.edu (T.H. Kuehn), bielicki.2@osu.edu (J.M. Bielicki), saarm@ethz.ch (M.O. Saar).

https://doi.org/10.1016/j.geothermics.2020.101865
Received 31 March 2019; Received in revised form 16 April 2020; Accepted 20 April 2020

utilization, and storage (CCUS) approach. In this type of CCUS, the geothermally heated CO_2 is produced through a well from the (geothermal) reservoir, expanded in a turbine to generate electricity, cooled, and reinjected through another well back into the reservoir, forming a closed loop, so that all of the CO_2 ultimately remains stored underground. Thus, some of the CO_2 molecules are utilized (to extract geothermal heat and to spin a turbine) and all of them are eventually stored underground, so that this is a true combined CCUS technology. The use of CO_2 was initially proposed as a geologic heat extraction fluid for Enhanced or Engineered Geothermal Systems (EGS) by Brown (2000), with subsequent modeling studies illustrating the effectiveness of such a CO_2-EGS approach (Atrens et al., 2010, 2009; Pruess, 2008, 2006). Supercritical CO_2 (sCO_2) has several advantages over brine as a heat extraction fluid, including a substantially lower kinematic viscosity (i.e., greater fluid mobility), which results in much higher heat advection rates within reservoirs, everything else being equal (Adams et al., 2015, 2014; Brown W., 2000). In addition to the higher mobility of sCO_2, the density of sCO_2 is much more temperature-dependent than that of brine. The combination of these thermophysical characteristics can generate a vigorously convecting thermosiphon that can reduce or eliminate the need for operating fluid circulation pumps, because the density difference between the injection and the production wells drives the CO_2 circulation (Adams et al., 2015, 2014; Atrens et al., 2010, 2009; Brown W., 2000). Furthermore, CO_2, as well as the weak carbonic acid that forms when CO_2 is dissolved in water, has a low mineral solubility, even in carbonate reservoirs (Luhmann et al., 2014; Tutolo et al., 2015, 2014). This low mineral solubility limits the leaching and transport of (dissolved) minerals from the rock, and will likely reduce subsequent scaling in pipes and turbomachinery (Brown W., 2000), which is a significant challenge in brine-based geothermal systems (Bélteky, 1975; Boch et al., 2017, 2016a, 2016b).

A different concept uses CO_2 as a heat extraction fluid in naturally porous and permeable sedimentary basins (Randolph and Saar, 2011a, 2011b; Saar et al., 2012). The CO_2 Plume Geothermal (CPG) process differs from (CO_2-based) EGS (Brown W., 2000; Pruess, 2008, 2006), in part because EGS requires hydraulic stimulation (i.e., hydraulic fracturing or shearing) to increase the permeability of the low-permeability formation (Amann et al., 2018; Gischig et al., 2019). In addition, naturally permeable reservoirs are typically large and enable the storage of large amounts of CO_2, especially in comparison to the small sizes and porosities of artificially generated, fracture-based EGS reservoirs (Randolph and Saar, 2011b, 2011c).

Prior research on CPG systems has focused on the modeling of fluid mass and energy transfer in the geologic reservoir and on the electricity generation in a surface power plant — both of which have assumed dry CO_2, i.e. no water. Like prior investigations of CO_2-EGS (Pruess, 2008, 2006), many CPG studies have modeled an inverted 5-spot well pattern (Adams et al., 2015, 2014; Randolph and Saar, 2011a, 2011b), and showed that the CPG system can generate a strong thermosiphon (Adams et al., 2014), produce more power than a brine-based geothermal system (Adams et al., 2015), and that the power output is more dispatchable than variable wind and solar renewable energy technologies (Adams and Kuehn, 2012).

More recent reservoir studies of CPG have used radially axisymmetric systems, with a vertical injection well at the center and a circular horizontal production well at the top of the reservoir under the caprock (Garapati et al., 2015, 2014). These radial models included multi-fluid (CO_2-brine) algorithms that also simulated the displacement of brine by CO_2, yet the power generation models continued to simulate the behavior of dry CO_2 in the wells and the surface power plant.

As a result, most prior research on CPG has assumed that the working fluid, extracted from the geothermal reservoir, is pure, dry CO_2, despite the fact that the deep saline aquifers, typically envisioned for CPG, are filled with brine prior to the injection of CO_2 (unless oil or gas reservoirs are considered). Only some of the brine in these aquifers will be displaced by the injected CO_2. Furthermore, some water will dissolve into the emplaced CO_2, and some CO_2 will dissolve into the water phase and form (weak) carbonic acid near the interface of the CO_2 plume (Spycher et al., 2003). We refer to CO_2 that contains some dissolved water (H_2O) as "wet" CO_2. Additionally, it is worth noting that when wet CO_2 is considered in CPG systems the corrosive effects of carbonic acid must also be considered, with corrosion resistant linings required in the equipment.

The maximum solubility in the vertical production well occurs at the bottom, as the fluid enters from the reservoir, where temperatures and pressures are large. As the solution moves up the production well both the pressure and the temperature decrease, reducing the solubility of H_2O in CO_2. As the CO_2 is likely to be saturated with H_2O when it enters the production well, some of the dissolved H_2O will exsolve from the CO_2 during the upwards movement within the production well. The exsolution of water from the CO_2 is an exothermic process that results in the formation of free-phase (liquid) H_2O. Given typically sufficient CO_2 flow rates, this free-phase H_2O is then co-produced to the surface, along with the CO_2 phase. At the surface, prior to the turbine, the co-produced H_2O may need to be separated from the CO_2 stream, similar to how liquid H_2O is removed in steam turbines, as the high density H_2O droplets can impinge and erode the turbine blades (Ahmad et al., 2009). It should be noted, however, that some liquid water in the CO_2 turbine, such as water condensation in the turbine, is not expected to be of significant concern, as the density of the liquid H_2O varies between 2.3 to 10.7 times the density of sCO_2 in the turbine, depending on the reservoir conditions. Conversely, in steam turbines, the liquid water and steam densities differ by more than a factor of 1000, so that the impingement of the high-density water droplets can more easily erode the turbine blades, requiring limits to be placed on the amount of allowable liquid water. Therefore, and as recently discussed with turbine manufacturers, substantially larger mass fractions of liquid water in supercritical CO_2 than the ~6% previously suggested (Garapati et al., 2015) are likely acceptable. Nonetheless, H_2O separation is necessary eventually (i.e., possibly after the turbine) because the re-injection of free-phase liquid H_2O substantially decreases the effective permeability of the reservoir near the injection well (Garapati et al., 2015).

The primary objective of this study is to determine the temperature, pressure, and mass fraction of free-phase liquid H_2O that may be produced at the wellhead, due to exsolution from CO_2 in the production well (i.e., not due to free-phase liquid H_2O entering the production well from the reservoir), and its effect on the power generation of CPG systems for reservoir depths ranging from 2.5 km to 5.0 km and geothermal temperature gradients (geotherms) of 20 °C/km to 50 °C/km. To do so, we compare three different methods for calculating wellhead water content (from exsolution from CO_2) and compare them against the TOUGH2 (Pruess et al., 1999) well simulator, T2Well (Pan et al., 2011). Then, for each of these methods, we numerically model the change in power generation due to including exothermic H_2O exsolution from CO_2 during CPG power plant operation.

2. Methods

The wellhead temperature, pressure, and water mass fractions are calculated using three different wellbore numerical models. Each of these methods uses the mass-weighted average, shown in Equation 1, to calculate the bulk density of the fluid along the length of the well.

$$\rho_{bulk,i} = \rho_{CO2,\,Solution,i}\,(1 - \varphi_{H2OL,i}) + \rho_{H2OL,i}\,\varphi_{H2OL,i} \quad (1)$$

The three models differ in their approximation of the CO_2 wellbore bulk density, $\rho_{bulk,i}$, in the following ways:

I **Dry CO_2Only:** The fluid in the well is assumed to be pure CO_2 (i.e. $\varphi_{H2OL,i} = 0$ and $\rho_{CO2,Solution} = \rho_{CO2}$). The pure CO_2 density, ρ_{CO2}, is obtained from Span and Wagner (1996).

II **CO_2Solution Proxy:** The fluid in the well is assumed to be a mixture of water-saturated CO_2 and liquid H_2O (i.e. $\varphi_{H2OL} \geq 0$). The CO_2 density is assumed to be that of pure, dry CO_2 (i.e. $\rho_{CO2,Solution} =$

Table 1
Nomenclature.

Variables		y	Mole fraction in the CO_2-rich Phase [-]
A	Cross-sectional Area [m^2]	z	Elevation [m]
D	Diameter [m]	η	Efficiency [-]
E	Energy [kJ]	ρ	Density [kg/m^3]
$\dot{E}$	Energy Rate [kW]	φ	Mass Fraction [-]
f	Darcy Friction Factor [-]	χ	Vapor Quality [-]
g	Gravitational Constant [m/s^2]		
h	Specific Enthalpy [kJ/kg]	*Subscripts*	
h_m	Molar Specific Enthalpy [kJ/mol]	bulk	Mixture Fluid Property (i.e. CO_2 and Water)
L	Length [m]	CO_2	Pure CO_2
$\dot{m}$	Mass Flow Rate [kg/s]	CO_2,Solution	CO_2 Solution (i.e. CO_2 and Dissolved Water)
M	Molar Mass [g/mol]	i	Well Segment Iteration
n	Moles of Component [-]	H2O	Total Water (i.e. Dissolved and Free)
P	Pressure [Pa]	H2Ov	Water Dissolved in CO_2
T	Temperature [°C]	H2OL	Free, Liquid Water
V	Bulk Velocity [m/s]	Haar	Relation from Haar et al. (1984)
$\dot{W}$	Electric Power [kWe]	S&W	Relation from Span and Wagner (1996)
x	Mole Fraction in the H_2O-rich Phase [-]	Spyc	Relation from Spycher et al. (2003, 2005, or 2010)
X	Mole Fraction [-]	Total	Total Component in any State

ρ_{CO2}) and obtained from Span and Wagner (1996). The free liquid H_2O density, ρ_{H2OL}, is obtained from steam tables (Haar et al., 1984). We include the CO_2 Solution Proxy method in this paper, as this density approximation is commonly used in other simulations, such as the T2Well simulator.

III **Solution Density Approximation:** The fluid in the well is assumed to be a mixture of water-saturated CO_2 and liquid H_2O (i.e. $\varphi_{H2OL} \geq 0$). The CO_2 density, $\rho_{CO2,Solution}$, is found for the CO_2-H_2O solution from Spycher et al. (2003; 2005; 2010). The free liquid H_2O density, ρ_{H2OL}, is obtained from steam tables (Haar et al., 1984).

Table 1 contains our nomenclature. Equations 2 to 4 describe the individual density values needed for the bulk density calculation. In all cases, the bulk temperature and pressure of the element are used to find the fluid density.

$$\rho_{CO2,i} = f_{S\&W}(T_{bulk,i},\ P_{bulk,i}) \tag{2}$$

$$\rho_{H2O,L,i} = f_{Haar}(T_{bulk,i},\ P_{bulk,i}) \tag{3}$$

$$\rho_{CO2,Solution,i} = \begin{cases} \rho_{CO2}, & Dry\ CO_2\ (I)\ and\ CO_2\ Solution\ Proxy\ (II) \\ f_{Spyc}(T_{bulk,i},\ P_{bulk,i},\ \varphi_{H2OL,i}), & Solution\ Density\ Approximation\ (III) \end{cases} \tag{4}$$

The difference between the *CO_2 Solution Proxy* and the *Solution Density Approximation* models is in the way the density of the CO_2 component of the mixture ($\rho_{CO2\_Solution,i}$ in Equation 4) is calculated. The *CO_2 Solution Proxy* approximates the density of the CO_2 component as that of pure CO_2, while the *Solution Density Approximation* method obtains the density from the CO_2-H_2O solution model from Spycher et al. (2003; 2005). We did not use the *Solution Density Approximation* method outright to estimate the CO_2 solution density, as wellbore simulators, namely T2Well, commonly make the assumption that the CO_2 component density is pure CO_2.

We employ a finite volume method with a numerical solver, namely Engineering Equation Solver (EES) by Klein and Alvarado (2002), to calculate the well fluid properties as a function of the height above the reservoir. This procedure is based on a prior approach that we developed for dry CO_2 (Adams et al., 2015, 2014). The well is divided into 100 m vertical elements to balance computational time and accuracy—as 100 m elements yield < 1% convergence error (Adams et al., 2015). Across each element, the exit state (i+1) is calculated from the inlet state (i), where equations for energy (Equation 5), momentum (Equation 6), and mass balance (Equation 7) are applied.

$$h_{bulk,i} + gz_i \bullet \frac{1kJ}{10^3 J} = h_{bulk,i+1} + gz_{i+1} \bullet \frac{1kJ}{10^3 J} \tag{5}$$

$$P_{bulk,i} + \rho_{bulk,i} g z_i = P_{bulk,i+1} + \rho_{bulk,i+1} g z_{i+1} - \Delta P_{loss,i} \tag{6}$$

$$\dot{m}_{Total,i} = \rho_{bulk,i} A_{pipe} V_{bulk,i} = \rho_{bulk,i+1} A_{pipe} V_{bulk,i+1} \tag{7}$$

Frictional pressure losses are determined from the Darcy-Weisbach relation (Equation 8).

$$\Delta P_{loss,i} = f \frac{L_{pipe}}{D} \rho_{bulk,i} \frac{(V_{bulk,i})^2}{2} \tag{8}$$

The friction factor, *f*, is given by the Moody Chart (Moody, 1944), using bare Cr13 oil piping, which has a surface roughness of $\varepsilon = 55\ \mu m$ (Farshad et al., 2010). We model the dynamic viscosity of the fluid as dry CO_2 in all three models, because CO_2 dominates the total mass fraction in the production well.

The model assumes no heat transfer between the well and the surrounding rock. Also, the model does not account for kinetic energy changes, as they are negligible (Adams et al., 2015, 2014; Randolph et al., 2012). For example, the largest wellbore velocity we observed was 2.2 m/s at the wellhead when simulating a 5 km deep reservoir. At this maximum velocity, the kinetic energy of the fluid ($V^2/2$) is 2.4 J/kg and the potential energy change of the fluid between the top and the bottom of the well ($g \bullet \Delta z$) is 49050 J/kg. Thus, the ratio of maximum kinetic energy change to potential energy change is 0.005% and the contribution of kinetic energy in the overall energy balance can be safely neglected.

We simulate the downhole reservoir-fluid pressure as hydrostatic and the downhole fluid temperature as the reservoir temperature, which is assumed to be the product of the geothermal temperature gradient and reservoir depth, added to an assumed mean annual surface temperature of 15 °C.

2.1. CO_2-H_2O Solution (Wet CO_2)

When CO_2 is injected into a brine reservoir, the mutual solubility of CO_2-H_2O has two effects: 1) CO_2 dissolves into the native brine and 2) H_2O dissolves and vaporizes into the CO_2-rich plume. The mutual solubility of the CO_2-H_2O system is defined by the phase and chemical equilibria equations. These are Equation 6, describing the transition of the gaseous phase CO_2 to the aqueous phase and Equation 10, describing the vaporization of water (Chen et al., 1992; Spycher et al., 2003; Spycher and Pruess, 2010, 2005).

$$CO_{2(g)} \rightleftharpoons CO_{2(aq)} \tag{9}$$

$$H_2O_{(l)} \rightleftharpoons H_2O_{(g)} \tag{10}$$

The solution properties of CO_2-H_2O mixtures for the pressures and temperatures encountered during geological CO_2 sequestration, and thus CPG systems, are defined by Spycher et al. (2003). This model was

extended to include the mutual solubility of CO_2-H_2O and CO_2-H_2O-NaCl systems in Spycher et al. (2005; 2010). These CO_2-H_2O models cover the temperature range 12-300 °C and pressure range 1-600 bar.

We assume that there is no NaCl present in any CO_2-H_2O solution. The presence of NaCl decreases the solubility of H_2O in CO_2. Thus, the resulting H_2O in CO_2 solubility, without NaCl, is an upper bound for the H_2O content possible under typical geothermal reservoir pressure and temperature conditions.

2.1.1. CO_2-H_2O Solution Energy Balance

The dissolved H_2O is assumed to be a saturated vapor, thus H_2O precipitation, or exsolution, as a free liquid, will transfer a substantial amount of energy to the CO_2 as it condenses. The assumption that dissolved water in CO_2 may be treated as vapor is further justified in Section 2.1.4.

Equation 10 indicates that the H_2O will undergo a phase change when the H_2O leaves the water-saturated CO_2. When H_2O exsolves from the H_2O-CO_2 solution, latent energy is released to the surrounding mixture. We neglect other chemical mixing processes and instead assume that the enthalpy of mixing is only due to the state change of pure water. In our model, the enthalpy of mixing is the energy required to transition saturated water vapor at the mixture temperature to liquid at the mixture temperature and pressure.

The CO_2 is assumed to be fully saturated with H_2O when the reservoir fluid enters the production well, with no free-phase H_2O present. Free-phase H_2O later develops as the fluid ascends within the well and the solubility of H_2O in CO_2 decreases and H_2O is forced out of solution due to the decrease in temperature and pressure. The energy, momentum, and continuity balances are expanded to include each of the three components: (1) CO_2, (2) the H_2O dissolved in the CO_2, and (3) free-phase H_2O present around the CO_2.

In Equations 11–14, the energy balance from Equation 5 is calculated separately for each component of the fluid: the CO_2 (CO2,i), H_2O in solution (H2Ov,i), and free liquid H_2O (H2OL,i). The temperature and pressure throughout each element (i) are assumed constant (i.e. bulk temperature, $T_{bulk,i}$, and pressure, $P_{bulk,i}$). The CO_2 (CO2,i) properties are evaluated at the bulk temperature and pressure (Equations 2,4, and 15). The H_2O in solution (H2Ov,i) is evaluated as a saturated vapor (i.e. $\chi = 1$) at the bulk temperature (Equation 16). The free liquid H_2O (H2OL,i) properties are evaluated at the bulk temperature and pressure (Equations 3 and 17). While the mass and energy of each component across a vertical well element can change (i.e. dissolved H_2O vapor becomes free-phase liquid, which increases the mass of liquid water and reduces the mass of dissolved vapor), the overall energy of the fluid must remain constant (Equation 11). We note that turbulent flow, and non-equilibrium thermodynamics may occur in the well, however, we assume a thermodynamic equilibrium model to illustrate a first-order approximation of the effect that H_2O solubility has on fluid states.

$$0 = \Delta\dot{E}_{CO2} + \Delta\dot{E}_{H2Ov} + \Delta\dot{E}_{H2OL} \tag{11}$$

$$\Delta\dot{E}_{CO2} = \dot{m}_{CO2,i+1}\left(h_{CO2,i+1} + gz_{i+1}\bullet\frac{1kJ}{10^3J}\right) - \dot{m}_{CO2,i}\left(h_{CO2,i} + gz_i\bullet\frac{1kJ}{10^3J}\right) \tag{12}$$

$$\Delta\dot{E}_{H2Ov} = \dot{m}_{H2Ov,i+1}\left(h_{H2Ov,i+1} + gz_{i+1}\bullet\frac{1kJ}{10^3J}\right) - \dot{m}_{H2Ov,i}\left(h_{H2Ov,i} + gz_i\bullet\frac{1kJ}{10^3J}\right) \tag{13}$$

$$\Delta\dot{E}_{H2OL} = \dot{m}_{H2OL,i+1}\left(h_{H2OL,i+1} + gz_{i+1}\bullet\frac{1kJ}{10^3J}\right) - \dot{m}_{H2OL,i}\left(h_{H2OL,i} + gz_i\bullet\frac{1kJ}{10^3J}\right) \tag{14}$$

$$h_{CO2,i} = f_{S\&W}\left(T_{bulk,i},\ P_{bulk,i}\right) \tag{15}$$

$$h_{H2Ov,i} = f_{Haar}\left(T_{bulk,i},\chi{=}1\right) \tag{16}$$

$$h_{H2OL,i} = f_{Haar}\left(T_{bulk,i},\ P_{bulk,i}\right) \tag{17}$$

2.1.2. CO_2-H_2O Solution Mass Balance

The total mass flow rate is the sum of the mass flow rates for CO_2, H_2O in solution, and liquid H_2O (Equation 18). The total mass flow rate must be constant across segments (Equation 7).

$$\dot{m}_{Total,i} = \dot{m}_{CO2,i} + \dot{m}_{H2Ov,i} + \dot{m}_{H2OL,i} \tag{18}$$

In addition, the mass flow rates of CO_2 and H_2O must be conserved between vertical well segments (Equations 19 and 20). For example, a decrease of H_2O solubility in CO_2 across one well element results in an increase of free water and a decrease of water in solution in the next segment, but the total mass of water is conserved (Equation 20).

$$\dot{m}_{CO2,i+1} = \dot{m}_{CO2,i} \tag{19}$$

$$\dot{m}_{H2O,Total} = \dot{m}_{H2Ov,i} + \dot{m}_{H2OL,i} = \dot{m}_{H2Ov,i+1} + \dot{m}_{H2OL,i+1} \tag{20}$$

Lastly, as the CO_2 is assumed to be fully saturated with H_2O in each element, the mass of dissolved water vapor is determined using the solubility limit from Spycher et al. (2003; 2005) (Equation 21) and converted from molar to mass units in Equation 22. It is represented as the free-phase liquid water mass fraction in Equation 23.

$$y_{H2O,MAX,i} = f_{spyc}\left(T_{bulk,i},\ P_{bulk,i}\right) \tag{21}$$

$$y_{H2O,MAX,i} = \frac{\frac{\dot{m}_{H2Ov,i}}{M_{H2O}}}{\frac{\dot{m}_{CO2,i}}{M_{CO2}} + \frac{\dot{m}_{H2Ov,i}}{M_{H2O}}} \tag{22}$$

$$\varphi_{H2OL,i} = \frac{\dot{m}_{H2OL,i}}{\dot{m}_{Total,i}} \tag{23}$$

2.1.3. Multi-component Solution Procedure

The wellbore fluid elements are solved numerically, from bottom to top. There are three steps to this procedure.

1 **Solve for Initial Conditions**. Using the initial conditions of produced fluid from the reservoir: $T_{bulk,0}$, $P_{bulk,0}$, z_0, $\dot{m}_{Total,0} = 100$ kg/s, and $\dot{m}_{H2OL,0} = 0$ kg/s, solve for the initial values of: $y_{H2O,MAX,0}$, $\dot{m}_{CO2,0}$, $\dot{m}_{H2Ov,0}$, $h_{CO2,0}$, $h_{H2Ov,0}$, $h_{H2OL,0}$, and $\varphi_{H2OL,0}$ using Equations 15,16,17,18,21,22, and 23. The initial bulk temperature and pressure are given by the reservoir depth, z_0, and geologic temperature gradient.

2 **Set up a For-loop.** The loop will increment in $N = z_0/\Delta z$ steps through the vertical elements. With each step, the elevation, z, increments by Δz. Here, we use an elevation step increment of $\Delta z = 100$ m. For a 2500 m deep well, this results in 25 steps. In the equations with both i and $i+1$ subscripts, the value from the previous step is given by i, while $i+1$ is the current value being solved.

3 **Solve the System of Equations in each Step.** The system of equations is given by 19 Equations: 1, 2, 3, 4, 6, 7, 8, 11, 12, 13, 14, 15, 16, 17, 18, 19, 21, 22, and 23. There are likewise 19 unknown variables: $T_{bulk,i}$, $P_{bulk,i}$, $y_{H2O,MAX,i}$, $\varphi_{H2OL,i}$, $\dot{m}_{CO2,i}$, $\dot{m}_{H2Ov,i}$, $\dot{m}_{H2OL,i}$, $h_{CO2,i}$, $h_{H2Ov,i}$, $h_{H2OL,i}$, $\Delta\dot{E}_{CO2,i}$, $\Delta\dot{E}_{H2Ov,i}$, $\Delta\dot{E}_{H2OL,i}$, $\rho_{CO2,i}$, $\rho_{CO2,Solution,i}$, $\rho_{H2OL,i}$, $\rho_{bulk,i}$, $V_{bulk,i}$, and $\Delta P_{loss,i}$. This system needs to be iteratively solved due to the several implicit functions. Here, we solve with EES, however, any software with similar capabilities, such as Nonlinear Equation System Solver (NESS) (Walsh et al., 2017) or MATLAB, could be used.

2.1.4. Enthalpy Model Validation

A fundamental assumption of our model is that water is dissolved as a vapor in the CO_2 and, therefore, will release energy as it exsolves out of solution as liquid water (Equation 10). An alternative modeling assumption would be that little energy change occurs when the solubility

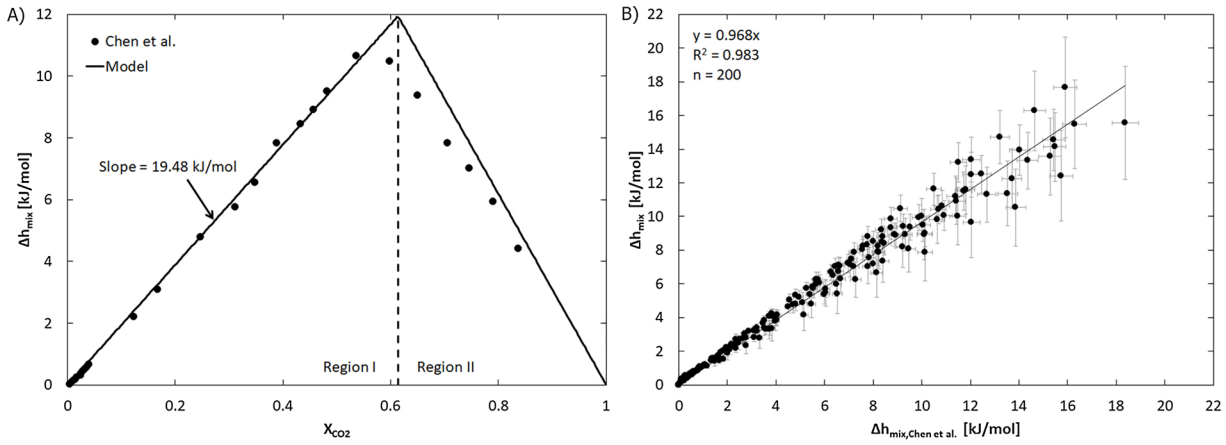

Fig. 1. The correlation of our modelled enthalpy of mixing with experimental data (Chen et al., 1992). A) At a single pressure and temperature of 12.4 MPa and 250 °C (with a solubility limit of $y_{H2O,MAX} = 0.387$). The transition between Regions I and II occurs at $X_{CO2} = 0.613 = 1 - 0.387$. B) The Region I agreement between our enthalpy of mixing model and experimental data for all temperatures and pressures reported by Chen et al. (1992).

changes and it therefore may be neglected (e.g. the assumptions of T2Well). As our vapor-water assumption is the primary driver for our results, we next validate this enthalpy modeling assumption with existing data.

Validation of our model over the entire range we simulate (25 to 50 MPa at 65 to 265 °C) is not possible because the published enthalpy of mixture values are limited for CO_2-H_2O systems. However, Chen et al. (1992) published experimentally determined enthalpy of mixture values for the CO_2-H_2O system from 225 to 325 °C at 10.4 to 15 MPa. Chen et al. (1992) reported the change in enthalpy as the specific enthalpy of mixing, Δh_{mix} [kJ mol^{-1}], for given values of the total mole fraction of CO_2 in the mixture, X_{CO2}. Here, we attempt to fit our enthalpy of mixing model to their results. Our hypothesis is that the observed enthalpy of mixing can be explained by the vaporization of water into the CO_2-rich phase. We develop a model which accounts for this vaporization and compare it with the data in Chen et al. (1992) to validate our assumption.

The specific enthalpy of mixing is defined by Chen et al. (1992) as the change in energy of a fixed number of moles of the mixture from its pure substances, divided by the total moles (Equation 24).

$$\Delta h_{mix} = \frac{E_{mixture} - E_{pure}}{n_{CO2} + n_{H2O}} \tag{24}$$

Here the total energy of the pure substances is the sum of the molar enthalpies of CO_2 and liquid water (Equation 25).

$$E_{pure} = n_{CO2} h_{m,CO2} + n_{H2O} h_{m,H2OL} \tag{25}$$

Our model makes the assumption that the total energy of the mixture is the sum of CO_2, liquid water, and dissolved water vapor energies (Equations 11–14), expressed in molar units Equation 26.

$$E_{mixture} = n_{CO2} h_{m,CO2} + n_{H2Ov} h_{m,H2Ov} + n_{H2OL} h_{m,H2OL} \tag{26}$$

We assume that the mole fraction of aqueous CO_2 is negligible (i.e. $x_{CO2} \approx 0$) as the solubility of CO_2 in water is less than 2% over the range of temperatures and pressures that we examine. We also assume that CO_2 has the same energy, regardless of whether it is a solute or solvent (i.e. gaseous or aqueous).

The number of moles of H_2O is the sum of moles in its different phases (Equation 27).

$$n_{H2O} = n_{H2OL} + n_{H2Ov} \tag{27}$$

Combining Equations 24 through 27 and eliminating terms yields Equation 28. The molar enthalpy of liquid water, $h_{m,H2OL}$, is evaluated at the temperature and pressure of the mixture. The molar enthalpy of water vapor, $h_{m,H2Ov}$, is evaluated as a saturated vapor at the mixture temperature.

$$\Delta h_{mix} = \frac{n_{H2Ov}}{n_{CO2} + n_{H2O}} (h_{m,H2Ov} - h_{m,H2OL}) \tag{28}$$

For the CO_2-rich phase, the solubility of H_2O in the CO_2, y_{H2O}, is the moles of dissolved water, assumed here to be vapor, divided by the total moles of CO_2 and H_2O vapor (Equation 29).

$$y_{H2O} = \frac{n_{H2Ov}}{n_{CO2} + n_{H2Ov}} \tag{29}$$

The total mole fraction of CO_2 in the mixture, X_{CO2}, is the moles of CO_2 divided by the total moles in the mixture (Equation 30).

$$X_{CO2} = \frac{n_{CO2}}{n_{CO2} + n_{H2O}} \tag{30}$$

Combining Equations 28 to 30 yields a specific enthalpy of mixing relationship, which is a function of CO_2 mole fraction, X_{CO2}, water solubility in CO_2, y_{H2O}, and the enthalpy difference of water, ($h_{m,H2Ov} - h_{m,H2OL}$). We use this relationship (Equation 31) to explain the data of Chen et al. (1992).

$$\Delta h_{mix} = X_{CO2} \frac{y_{H2O}}{1 - y_{H2O}} (h_{m,H2Ov} - h_{m,H2OL}) \tag{31}$$

A mixture of CO_2 and H_2O has two regions, one "CO_2-limited," where there is excess water and any CO_2 is fully saturated with H_2O (Region I), and one "H_2O-limited," where there is excess CO_2 and the CO_2 contains H_2O at concentrations below its solubility limit (Region II). Fig. 1A shows these two regions with data from Chen et al. (1992) for a pressure of 12.4 MPa and a temperature of 250 °C. At this temperature and pressure, the solubility limit is $y_{H2O,MAX} = 0.387$ from Spycher et al. (2003; 2010; 2005). In addition, at this temperature and pressure, the difference in enthalpy between vapor and liquid H_2O, ($h_{m,H2Ov} - h_{m,H2OL}$), is 30.9 kJ mol^{-1}.

At a CO_2 mole fraction of $X_{CO2} = 0$, the system is pure water. As the CO_2 mole fraction increases through Region I, the dissolved water mass increases, requiring more vaporization of water, thereby increasing the enthalpy of mixing. Once the full saturation point is reached at $X_{CO2} = 1 - y_{H2O,MAX}$, all H_2O has been dissolved into CO_2 and there is no excess water. This occurs at $X_{CO2} = 0.613$ in Fig. 1A. As the CO_2 fraction is increased into Region II, there is insufficient H_2O present to fully saturate the CO_2. Consequently, the fraction of H_2O in the CO_2, y_{H2O}, decreases below the saturation point, so that the amount of vaporized water decreases, decreasing the enthalpy of mixing.

$$\Delta h_{mix} = \begin{cases} X_{CO2} \dfrac{y_{H2O,MAX}}{1 - y_{H2O,MAX}} (h_{m,H2Ov} - h_{m,H2OL}) \text{(Region I)} \\ (1 - X_{CO2})(h_{m,H2Ov} - h_{m,H2OL}) \text{(Region II)} \end{cases} \tag{32}$$

Equation 32 provides the enthalpy of mixing relationships, modified from Equation 31, for Regions I and II, respectively. In Region I, the CO_2 is always fully saturated with H_2O ($y_{H2O} = y_{H2O,MAX}$). In Region II, the H_2O in CO_2 is below the saturation limit. As we assume that there is no CO_2 dissolved in H_2O ($x_{CO2} \approx 0$) and all the water is dissolved in CO_2, the CO_2 mole fraction is equal to one minus the mole fraction of H_2O in CO_2, i.e., $X_{CO2} = 1 - y_{H2O}$. Thus, Equation 31 further reduces in Equation 32 for Region II. Equation 32 is plotted as lines in Fig. 1A.

The enthalpy of mixing values are plotted against the CO_2 mole fractions in Fig. 1A. In Region I, these values form a line with a slope of 19.48 kJ mol^{-1}, which is the first derivative of Equation 32.

Fig. 1B shows the correlation between our Region I enthalpy of mixing model (Equation 32) and the data reported by Chen et al. (1992) for all their investigated temperatures and pressures. A correlation of $R^2 = 1$ and a slope of 1 would indicate a perfect agreement between the models. The resulting slope and coefficient of determination (R^2) are 0.968 and 0.983, respectively, for our model (Equations 24–32), thus our model accounts for 98.3% of the data variation but underestimates their values by ~3%. The variation between the experimental values and the model is within the 5% uncertainty in the soluble H_2O mole fraction, y_{H2O}, reported by Spycher et al. (2005), indicated by the vertical error bars in Fig. 1B. Additionally, the 3% experimental variations reported by Chen et al. (1992) are indicated by the horizontal error bars in Fig. 1B.

In Region II, the mole fraction of water is insufficient to fully saturate the CO_2 and y_{H2O} decreases below the saturation limit, $y_{H2O,MAX}$. This relationship between the CO_2 fraction and the enthalpy of mixing is given by Equation 32, where the slope is the negative of the difference of H_2O enthalpies (-30.9 kJ mol^{-1}).

While our model fits the data quite well in Region I, it overestimates the enthalpy of mixing in Region II. It is possible that in this region, not all the water enters the solution and some water remains as a liquid, which is not accounted for in our model. Additionally, allowing for CO_2 dissolution in water (i.e. $x_{CO2} > 0$) would reduce the available CO_2 and more closely align the model to the data. However, in the wellbore model, used in this paper, the CO_2 is always fully saturated with H_2O, so that we are chiefly concerned with the data fit in Region I. Thus, our assumption that the enthalpy of mixing is primarily determined by the vaporization and condensation of water into fully-saturated CO_2 is validated here.

In this section, we have shown that the enthalpy of mixing may be approximated by the enthalpy difference between water liquid and vapor for a CO_2-H_2O solution, and validated this assumption using data from Chen et al. (1992). Therefore, our assumption that dissolved water in CO_2 may be modeled as saturated vapor is justified.

2.2. TOUGH2 Simulator Model

Our results are compared with results we obtain employing the standard well flow simulator TOUGH2 T2Well (Pan et al., 2011, 2009). T2Well (Pan et al., 2011) uses the TOUGH2 (Pruess et al., 1999) numerical simulator with the TOUGH2-ECO2N (Pruess, 2005) equation of state module. The T2Well-ECO2N module incorporates the thermodynamic properties of the CO_2-H_2O-NaCl system, but the ECO2N module is limited to the temperature range from 12 to 110 °C, which is a subset of the parameter space investigated here. Thus, the T2Well simulator results can only be compared to our results, where they are also valid.

The T2Well simulator differs from our model in three ways. First, it uses a transient drift-flux model (DFM) to simulate the flow rates and pressure losses of the two-phase flow of CO_2-H_2O mixtures (Pan et al., 2009). In contrast, our model assumes a single, homogenous flow with a single bulk density and velocity. As the fraction of liquid water is small for the cases considered here, the inclusion of the DFM modeling approach is not expected to produce appreciable differences from our bulk flow models. Second, unlike our approach, the ECO2N module does not include the change in fluid enthalpy as the water exsolves from CO_2 to free-phase liquid water. Instead, the ECO2N module assumes that the CO_2, with H_2O in solution, has the thermodynamic properties of dry CO_2. Third, the T2Well simulator numerically integrates, using 10-meter segments along the axis of the well, whereas we use 100-meter well segments. This difference in well segment length is negligible, as our previous study has found that 100-meter well segments result in less than 1% discretization error from much shorter well segments (Adams et al., 2014).

Thus, the T2Well simulator differs primarily from our simulations of water-saturated CO_2 in that it neglects the heat of vaporization of water as the water exsolves from CO_2 in the wellbore. Therefore, we expect the results of the T2Well model to agree most closely with our simulations for the dry CO_2 cases.

2.3. Power Plant Sensitivity Model

The surface power plant model determines the change in electric power generated from a direct CO_2-Plume Geothermal (CPG) system that uses water-saturated (i.e. wet) CO_2 instead of the pure, dry CO_2 that we used in our previous work (Adams et al., 2015, 2014). The direct CPG system generates power by directly expanding the produced CO_2 in a turbine, as opposed to the less efficient binary cycle, where heat is transferred to a secondary working fluid to generate power (Adams et al., 2015). Wet CO_2 will affect the power generated due to the change in two principal system parameters: 1) the temperature and pressure of the fluid at the wellhead and 2) the mass flow rate of CO_2 that passes through the turbine, provided that free-phase liquid water is removed at the wellhead, before the turbine.

In this power model, we assume conservatively that any produced liquid water will be separated from the wet CO_2 before the turbine, thereby reducing the mass flow rate through the turbine (Fig. 2). Conventional tank separation methods are assumed for the separation of fluids. As these are relatively simple devices, allowing the different phases, with differing densities, sufficient time to separate, in principle, they do not require power to operate. Thus, the energy required to remove the water is neglected (Hansen et al., 1993; Simmons et al., 2002). Additionally, the water separator is assumed to be isobaric and isothermal.

To estimate the effect of wet CO_2 on power generation, the turbine power, $\dot{W}_{turbine}$, is numerically simulated with Engineering Equation Solver (EES) for each of the four well models, namely 1) *Dry CO_2 Only*, 2) *CO_2 Solution Proxy*, 3) *Solution Density Approximation*, and 4) T2Well, which are presented in Section 2.0. Consistent with our earlier work (Adams et al., 2015), we assume an $\eta = 78\%$ isentropic turbine efficiency (Equation 33).

$$\eta = \frac{(h_{in} - h_{out})}{(h_{in} - h_{out,isentropic})} \tag{33}$$

The power generated by an adiabatic turbine is the product of the mass flow rate and the difference between the enthalpy of the fluid at the turbine inlet and exit (Equation 34). The fluid flowing through the turbine is assumed to be pure CO_2.

$$\dot{W}_{turbine} = \dot{m}_{turbine}(h_{in} - h_{out}) \tag{34}$$

In the dry CO_2 case, the mass flow rate through the turbine is equal to the mass flow rate in the well and there is no need for a separator. When free-phase liquid water is separated from the produced fluid, the fluid (then just CO_2) mass flow rate through the turbine is reduced by the fraction of water, ϕ_{H2OL}, that is removed from the produced fluid (Equation 35).

$$\dot{m}_{turbine} = \dot{m}_{total}(1 - \varphi_{H2OL}) \tag{35}$$

The turbine inlet enthalpy is found using the wellhead fluid pressure and temperature, which change when wet CO_2 is considered. As a result, the fraction of turbine power change, due to the wet CO_2, relative

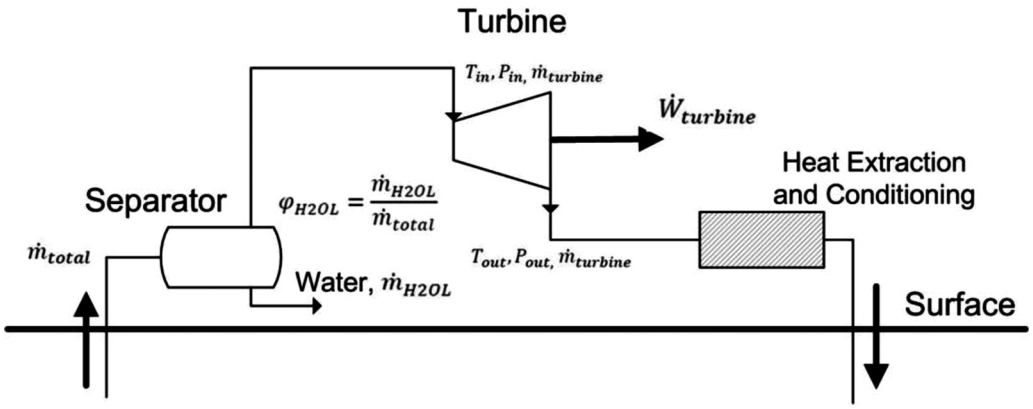

Fig. 2. Schematic of the surface component of a CO_2-Plume Geothermal (CPG) power plant that includes liquid water separation at the surface, where $\dot{m}_{Total}$ is the total mass flow rate of the produced multi-phase fluid and $\dot{m}_{H2OL}$ is the mass flow rate of liquid water. All other parameters are defined in the main text and in Table 1.

to the turbine power when using dry CO_2, is given by Equation 36.

$$\frac{\Delta \dot{W}}{\dot{W}} = (1 - \varphi_{H2OL}) \frac{(h_{in,wet} - h_{out,wet})}{(h_{in,dry} - h_{out,dry})} - 1 \quad (36)$$

The turbine inlet enthalpy, h_{in}, is calculated from the temperature and pressure at the wellhead. The exit enthalpy, h_{out}, is calculated using the isentropic turbine efficiency. The isentropic outlet enthalpy, $h_{out,isentropic}$, is the enthalpy at the state defined by the inlet entropy and an exit pressure equal to the saturation pressure of CO_2 at a temperature of 22 °C (6.03 MPa), similar to Adams et al. (2015).

3. Application and Results

The results are described in three parts: a single comparison case, a parametric study, and a power generation sensitivity analysis. A single case is used first to illustrate the differences between each of the well models. Then, the impact of wet CO_2 on wellhead temperature and pressure is found for a range of reservoir depths from 2.5 km to 5.0 km and for geothermal temperature gradients from 20 °C/km to 50 °C/km. Lastly, we employ a power generation sensitivity analysis to estimate the change in surface plant power generated due to the exsolution of water from CO_2.

3.1. Single Comparison Case

This comparison is conducted employing values from the base case, described in Adams et al. (2015), where the total production fluid mass flow rate is 100 kg/s, the production well depth is 2.5 km, the geothermal temperature gradient is 35 °C/km, and the mean annual surface temperature is 15 °C. Thus, the downhole reservoir temperature is 102.5 °C and the fluid pressure in the reservoir is hydrostatic, at 25 MPa. We assume a production well diameter of 0.41 meters. The results are summarized in Fig. 3 in terms of pressure, temperature, and liquid H_2O mass fraction.

The wet CO_2-H_2O models predict higher wellhead pressures and temperatures than the pure CO_2 case, as shown in Fig. 3A and B. Both exsolution models, the *CO_2 Solution Proxy* and *the Solution Density Approximation*, result in substantially larger increases in the wellhead pressure and temperature than the T2Well and dry CO_2 models. In both of these cases, the temperature increase is from the inclusion of the exothermic exsolution of H_2O in the model, with the released energy increasing the fluid temperature relative to the pure CO_2 and T2Well cases. The increased fluid temperature, in turn, reduces the density of the CO_2 and the bulk fluid density, resulting in higher pressures in the wellbore. The T2Well model is similar to the dry CO_2 case, with slightly elevated pressures and temperatures, as this model excludes the exothermic exsolution of CO_2. Thus, including the exsolution of H_2O in the model has a substantial impact on the wellbore pressure and temperature profiles.

The pressure and temperature differences between the *CO_2 Solution Proxy* and *Solution Density Approximation* models illustrate the effect of varying the CO_2 solution density. The *CO_2 Solution Proxy* method approximates the solution density as that of pure CO_2 and, therefore, only differs from the T2Well and pure CO_2 methods by including the heat addition from the exothermic exsolution of H_2O. As a result, this method always has a bulk density less than the density of dry CO_2 in the well, indicated by the positive pressure profile in Fig. 3A. In contrast, the *Solution Density Approximation* model directly calculates the CO_2 component solution density, which can have densities greater than pure CO_2, even at elevated temperatures. This higher density is indicated in Fig. 3A by the negative pressure difference near the bottom of the vertical production well. In the 2.5 km, 102 °C base case, the density difference between these models is small, as the amount of H_2O in solution is small, and thus the production wellhead pressure and temperature are similar, varying by 0.1 MPa and 0.5 °C (zero depth in Fig. 3A and B).

Fig. 3C shows the percentage of free-phase liquid H_2O in the production well. As the fluid ascends in the well, its pressure and temperature decrease, which decreases the solubility of H_2O in CO_2, so that H_2O exsolves and forms free-phase water. All three solution models predict similar free liquid H_2O mass fractions as a function of well depth and use the same model to predict the H_2O saturation limit. Thus, the slight variation between each model is caused by the small differences in predicted wellbore pressure and temperature. It is worth noting, that the T2Well case has exsolved slightly more liquid H_2O by the time the production wellhead is reached, compared to the other models, as the T2Well model results in the lowest predicted wellhead pressure and temperature. Overall, this base case has a small amount of wellhead H_2O produced, 0.62% +/- 0.02%, because the downhole reservoir temperature and pressure are relatively low, minimizing the amount of H_2O that dissolves into CO_2, and thus minimizing the amount of dissolved H_2O entering the production wellbore. With less H_2O that can come out of solution, less H_2O is exsolved by the time the production wellhead is reached.

3.2. Parameter Space

We estimate the temperature, pressure, and free-phase H_2O mass fraction of the produced fluid for combinations of three reservoir depths (2.5 km, 3.5 km, and 5.0 km) and three geothermal temperature gradients (20 °C/km, 35 °C/km, and 50 °C/km). The mass flow rate of water-saturated CO_2, at the production well inlet (located at reservoir depth), is constant at 100 kg/s and is based on our previous work (Adams et al., 2015). The mean annual surface air temperature is 15 °C and the well diameter is 0.41 m. Table 2 shows the mass fraction of H_2O in solution entering the production well from the reservoir and the free-phase liquid H_2O at the production wellhead. Table 3 presents the fluid pressures and temperatures at the production well inlet and at the

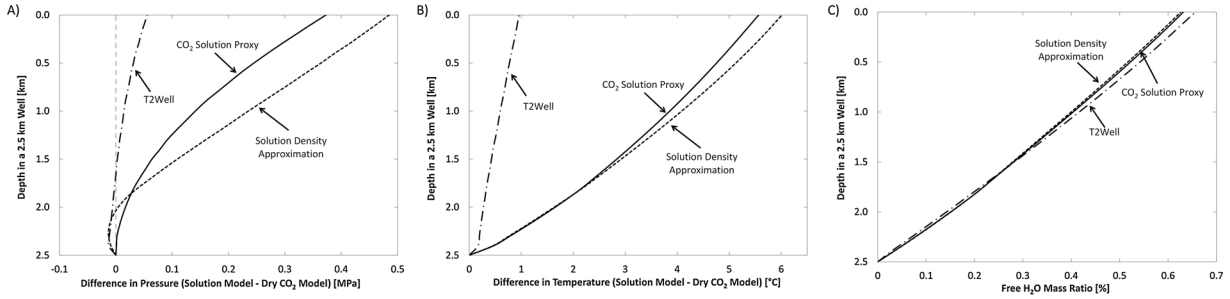

Fig. 3. Differences, for the base case, between each solution model and the pure CO_2 model over the length of the vertical production well for (A) fluid pressure, (B) temperature, and (C) the free-phase liquid water ratio. A positive difference indicates that the model predicts a greater value than the dry CO_2 model.

production wellhead.

Table 2 shows that the solubility of H_2O in CO_2 increases as the temperature and pressure of the fluid increase. The solubility of H_2O in CO_2 in the reservoir ranges from 0.42% in a 2.5 km deep, 65 °C reservoir to 19.01% in a 5.0 km deep, 265 °C reservoir.

At the wellhead, the produced mass fraction of liquid H_2O is generally low, despite the large mass fractions of H_2O that enters from the reservoir in the form of H_2O dissolved in CO_2, as H_2O tends to remain in solution with the CO_2. The fraction of liquid water produced at the wellhead varies between 0.28% for a 2.5 km deep, 65 °C reservoir and 3.98% for a 5.0 km deep, 265 °C reservoir. Additionally, in all but one case (the 5.0 km deep and 265 °C hot reservoir), the models predict production wellhead liquid water fractions less than 3%. In this study, we do not consider any free-phase liquid H_2O that may enter the production well from the reservoir, as such H_2O addition is expected to be minor for pore-space CO_2 saturations around the production well inlet of at least 40% (Buckley and Leverett, 1942). This minimum CO_2 saturation is assumed to be required to begin CPG operations (Garapati et al., 2015). Furthermore, the focus of our paper here is on quantifying the amount of extra power generation due to the exothermic exsolution of H_2O that entered the production well dissolved in CO_2.

The produced wellhead temperature for wet CO_2 is almost always greater than that of dry CO_2, and generally increases with the reservoir depth and geothermal temperature gradient, as shown in Table 3. This occurs because the exothermic exsolution of water from CO_2 during the ascent of the fluid in the production well increases the fluid temperature, as previously discussed. The notable exception to this is seen in the T2Well results, as T2Well neglects the enthalpy of exsolution and can thus result in wellhead temperatures that are lower than those predicted by the *Dry CO_2* model.

The wellhead pressure varies with the density assumptions for the wet CO_2 cases. The *CO_2 Solution Proxy* method always results in wellhead pressures greater than the dry CO_2, a result of assuming that the CO_2 component density is that of dry CO_2, while simultaneously allowing exothermic H_2O exsolution to heat the fluid. The *Solution Density Approximation* method results in increased wellhead pressures when the mass fraction of H_2O in solution is low (typically below 2%), which generally occurs at low geothermal temperature gradients and shallow reservoir depths. At larger mass fractions of H_2O in solution, the solution density increases, due to the dissolved H_2O, and the wellhead pressure is less than that of dry CO_2, despite the exsolution effects. Hence, the choice of the solution density model has a substantial impact on wellhead pressures and should thus be carefully chosen. Therefore, we recommend using the more complex *Solution Density Approximation* and reserve the *CO_2 Solution Proxy* only for approximations.

The mass fraction of H_2O in solution in CO_2, given by Spycher et al. (2003), has an uncertainty of 5%. When this error is propagated through our wellbore models, the resulting uncertainty in pressure and temperature at the production wellhead is less than 0.5% and the uncertainty in the produced free-phase liquid water at the production wellhead is 5%. Furthermore, the uncertainty in the power generated by the turbine (Section 3.3) is less than 1.1% for all cases.

3.3. Power Generation Sensitivity to Exsolved Water

The exsolution of water from CO_2 affects the electric power generation of a direct CO_2-Plume Geothermal (CPG) power plant in two important ways: 1) by reducing the CO_2 mass flow rate through the turbine, as we conservatively assume that the free-phase liquid water is removed before the fluid enters the turbine, and 2) by changing the wellhead fluid temperature and pressure. Thus, in this section, we investigate the change in power generation due to these processes.

Table 2
The mass fraction of water in the CO_2 solution, entering the production well, and the mass fraction of free-phase liquid water at the production wellhead for each well model for reservoir depths of 2.5, 3.5, and 5 km and geothermal temperature gradients of 20, 35, and 50 °C/km.

				Reservoir H_2O Mass Ratio (%)			Wellhead Liquid H_2O Mass Ratio (%)		
Reservoir Depth (km)	Reservoir Pressure (MPa)	Temperature Gradient (°C/km)	Reservoir Temperature (°C)	CO_2 Solution Proxy	Solution Density Approximation	T2Well	CO_2 Solution Proxy	Solution Density Approximation	T2Well
2.5	25	20	65.0	0.42	0.42	0.42	0.28	0.28	0.31
2.5	25	35	102.5	0.93	0.93	0.90	0.63	0.63	0.65
2.5	25	50	140.0	2.09	2.09	-	1.04	1.08	-
3.5	35	20	85.0	0.69	0.69	0.69	0.49	0.47	0.52
3.5	35	35	137.5	2.15	2.15	-	1.31	1.36	-
3.5	35	50	190.0	5.63	5.63	-	1.93	2.02	-
5.0	50	20	115.0	1.44	1.44	-	1.03	1.03	-
5.0	50	35	190.0	5.97	5.97	-	2.57	2.71	-
5.0	50	50	265.0	19.01	19.01	-	3.72	3.98	-

Table 3
Fluid temperatures and pressures at the production wellhead for each well model and for reservoirs depths of 2.5, 3.5, and 5 km and geothermal temperature gradients of 20, 35, and 50 °C/km.

				Pressure (MPa)				Temperature (°C)			
Reservoir Depth (km)	Reservoir Pressure (MPa)	Temperature Gradient (°C/km)	Reservoir Temperature (°C)	Dry CO_2	CO_2 Solution Proxy	Solution Density Approximation	T2Well	Dry CO_2	CO_2 Solution Proxy	Solution Density Approximation	T2Well
2.5	25	20	65.0	7.62	7.85	8.25	7.72	31.4	32.7	34.1	31.2
2.5	25	35	102.5	12.28	12.64	12.75	12.34	61.4	66.8	67.3	62.8
2.5	25	50	140.0	15.29	15.61	15.17	-	100.7	113.9	112.7	-
3.5	35	20	85.0	10.68	11.11	11.60	10.80	43.2	46.7	48.1	44.3
3.5	35	35	137.5	16.90	17.62	16.92	-	89.1	104.0	102.3	-
3.5	35	50	190.0	20.77	21.31	20.27	-	144.1	170.6	169.3	-
5.0	50	20	115.0	15.43	16.46	16.52	-	62.1	72.1	72.2	-
5.0	50	35	190.0	23.97	25.20	23.39	-	132.5	165.9	164.2	-
5.0	50	50	265.0	29.09	29.86	25.99	-	211.1	257.4	256.0	-

The electric power output of a turbine is given by the product of the mass flow rate and the enthalpy drop across the turbine (Equation 34). As mentioned before, we assume an isentropic turbine efficiency of 78%. The exsolution of water from wet CO_2 alters the fluid state at the wellhead from that of dry CO_2, while the turbine outlet pressure remains fixed. Thus, the enthalpy difference across the turbine changes, which results in differences in turbine power output. Only the change in generated turbine power is considered here. Parasitic power, for example due to running pumps, compressors, fluid separation devices, or cooling fans is neglected. Separation power is assumed small and, thus, negligible, as described in the methodology section.

Table 4 and Fig. 4 show the increase in the electric power output from dry to wet CO_2 for the *CO_2 Solution Proxy*, the *Solution Density Approximation*, and the T2Well simulations. The produced water fraction values from Table 2 are used in Equations 33–36 to determine the change in the electric power output of the turbine.

Table 4 shows that wet CO_2, with liquid water removal, generates approximately 8% to 41% more electric power in a direct CPG system than dry CO_2, because, as described before, the exothermic exsolution of water from solution in CO_2 increases the production wellhead fluid enthalpy, that later increases the electric power generation by the turbine. This effect more than outweighs the reduction in power generation due to the decreased mass flow rates that result from our conservative assumption that the free-phase liquid water is removed before the turbine. It is worth noting that after the turbine generally over 95% of the produced H_2O exsolves from the solution, which is typically significantly larger than the exsolved fraction at the wellhead, thus liquid H_2O separation after the turbine may be required (in addition to any H_2O separation that occurred before the turbine to protect the turbine) to prevent H_2O reinjection, reducing the injectivity index, causing fluid and pressure buildup in the reservoir near the injection well (Garapati et al., 2015).

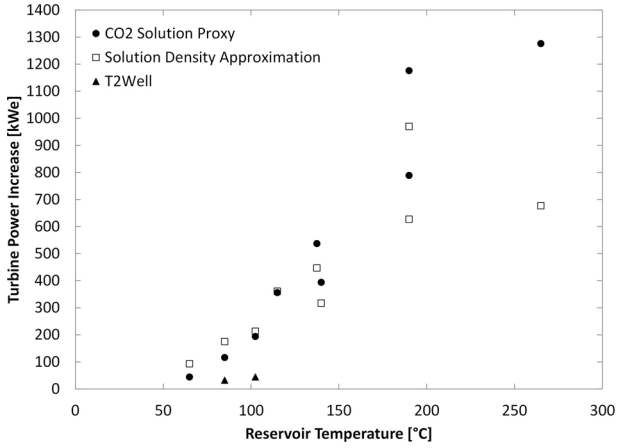

Fig. 4. Increase in the electric power output of the turbine due to exothermic water exsolution from water-saturated CO_2 during the ascent of wet CO_2 in the production well from geologic reservoirs of varying depths and associated temperatures for the three water solubility models considered in this study.

The T2Well model predicts less extra electricity generation than the wet exothermic exsolution models (i.e. the *CO_2 Solution Proxy* and the *Solution Density Approximation*). For example, at a reservoir depth of

Table 4
Turbine electric power output and its percent increase for the geologic reservoirs of varying depths and temperatures for the three water solubility models considered in this study.

				Turbine Power (KW_e)				$\Delta W/W_{dry}$ (%)		
Reservoir Depth (km)	Reservoir Pressure (MPa)	Temperature Gradient (°C/km)	Reservoir Temperature (°C)	Dry CO_2	CO_2 Solution Proxy	Solution Density Approximation	T2Well	CO_2 Solution Proxy	Solution Density Approximation	T2Well
2.5	25	20	65.0	226	270	319	225	19.48	41.21	−0.62
2.5	25	35	102.5	1344	1538	1557	1388	14.43	15.85	3.27
2.5	25	50	140.0	2798	3192	3115	-	14.08	11.33	-
3.5	35	20	85.0	665	781	840	697	17.55	26.44	4.91
3.5	35	35	137.5	2448	2985	2895	-	21.94	18.26	-
3.5	35	50	190.0	4608	5397	5235	-	17.12	13.61	-
5.0	50	20	115.0	1435	1791	1796	-	24.81	25.16	-
5.0	50	35	190.0	4381	5557	5351	-	26.84	22.14	-
5.0	50	50	265.0	7629	8905	8306	-	16.73	8.87	-

2.5 km and a geothermal temperature gradient of 35 °C/km, the T2Well model results estimate a 3.3% increase in power generation when switching from dry to wet CO_2, while the corresponding increase in power generation with the *CO_2 Solution Proxy* and the *Solution Density Approximation* models is 14.4% and 15.8%, respectively. This occurs because the T2Well model neglects the enthalpy of exsolution, which fundamentally decreases the produced CO_2 enthalpy.

It is worth noting that we include the results of the T2Well and the *CO_2 Solution Proxy* models here as they represent commonly used fluid density assumptions, made in numerical simulators. However, our results, discussed below, show that accurate fluid density models (i.e. the CO_2-H_2O equation of state in the *Solution Density Approximation*) are essential to calculate production wellhead fluid properties of CO_2-H_2O mixtures correctly.

The power generated is sensitive to the wellbore density model in the vertical well, particularly at high mass fractions of H_2O entering the well. At low H_2O mass fractions, generally below 2%, where the *Solution Density Approximation* and the *CO_2 Solution Proxy* methods yield similar CO_2 densities, the difference in the power generated between the wet and the dry CO_2 models generally increases with the mass fraction of H_2O. However, at larger H_2O mass fractions, the density yielded by the *Solution Density Approximation* method is higher than the *CO_2 Solution Proxy* method, resulting in lower wellhead pressures and thus reduced power generation. For instance, the turbine power increase for the 5 km deep, 265 °C reservoir case (with 19.01% H_2O mass fraction) varies between 8.9% and 16.7% solely due to the differences in the fluid density model employed. Thus, for high H_2O mass fractions entering the well (i.e. deep reservoir with high geologic temperature gradients), accurately modeling the solution density, as done in the *Solution Density Approximation*, is vital in determining the power generated in wet-CO_2 CPG systems. Additionally, it is worth noting that these density models only consider the CO_2-H_2O system and that any addition of other components would further alter the fluid density, requiring the consideration of all components dissolved in the production well CO_2 phase to accurately predict CPG power output.

Overall, the largest factor that causes differences in turbine power generation is the density of the production wellbore fluid. The *CO_2 Solution Proxy* model estimates a slightly lower fluid density than the *Dry CO_2* model, which results in higher wellhead fluid temperatures and pressures and, thus, more turbine power generation. Conversely, the *Solution Density Approximation* model provides approximately the same heat input, due to exsolving water, as the *CO_2 Solution Proxy*, however, the fluid density, determined by the *Solution Density Approximation* model, can be substantially lower or higher than that of dry CO_2, depending on the dissolved water content. When the wellbore fluid density is lower than that of dry CO_2, the production wellhead fluid pressure is larger and the *Solution Density Approximation* model predicts higher CPG electric power generation rates. Conversely, when the wellbore density of the *Solution Density Approximation* model is larger than that of dry CO_2, the same energy input results in lower wellhead fluid pressures and smaller increases in electric power generation. As such, the enthalpy of exsolution and the CO_2-H_2O solution density are fundamental components in the calculation of CO_2-Plume Geothermal (CPG) power generation and should not be neglected or substituted with the properties of dry CO_2.

4. Conclusions

Numerically modeling fluid mass and energy transfer in production wells as wet CO_2 (i.e., CO_2 with dissolved H_2O), instead of dry CO_2, can have a substantial impact on the wellhead fluid temperature and pressure. Here, we show in particular, how the consideration of water, first dissolved in CO_2 at the bottom of a production well and later partially, exothermally exsolving from the CO_2 as the fluid rises in the production well, can result in a substantial increase in the electric power generation capacity of direct CO_2-Plume Geothermal (CPG) power plants. The results of our numerical simulations, for reservoir depths of 2.5 km to 5.0 km and geothermal temperature gradients of 20 °C/km to 50 °C/km, suggest the following:

The inclusion of H_2O in solution with CO_2 leads to the production of free-phase liquid H_2O at the production wellhead, due to the exsolution of the initially dissolved H_2O during the upwards flow of the production fluid as it experiences a decrease in fluid pressure and temperature, reducing the solubility of H_2O in CO_2. Over the range of conditions we investigated, the downhole, wet CO_2 contains up to 19.2% dissolved H_2O by mass, depending on the temperature and pressure of the reservoir fluid, assuming that the reservoir CO_2 is fully saturated with H_2O. While the mass fraction of produced wellhead liquid H_2O is small for the majority of cases (< 2%), it can be as much as 4% in the 265 °C reservoir case.

The employed wet CO_2 models nearly always produce a higher wellhead fluid temperature than dry CO_2, due to the exothermic exsolution of H_2O from CO_2. When the enthalpy input to CO_2 from the exsolving and condensing H_2O is considered, all employed models yield wellhead fluid temperatures that are typically between 1.3 °C and 46.3 °C higher than when dry CO_2 is assumed in the production well.

For large mass fractions of H_2O in solution with CO_2, the multi-component density model of the Solution Density Approximation method is necessary. For H_2O mass fractions dissolved in CO_2 less than 1%, the CO_2-H_2O solution density can be modeled as dry CO_2 in the wellbore. At H_2O mass fractions greater than 1%, assuming the CO_2 component is dry CO_2 (*CO_2 Solution Proxy* method) yields substantially smaller fluid densities, which cause overestimations of wellhead fluid pressures and turbine power generation.

Considering water-saturated CO_2, entering the production well of CPG systems, increases the turbine electric power output, in the cases investigated, by 15% to 25% on average and up to a maximum of 41%, compared to when dry CO_2 is assumed. The higher production wellhead fluid temperatures and pressures, that result when using wet CO_2, increase the enthalpy difference across the turbine. This increase in electric power generation occurs despite our conservative estimate that the liquid water is removed at the wellhead, before the turbine, which reduces the mass flow rate through the turbine and thus the power generation. We note that this is the conservative estimate as some liquid H_2O is expected to be acceptable in the turbine, given that the density difference between liquid H_2O and the CO_2 is small in the turbine. However, the discussion of the acceptable liquid H_2O limit in a CO_2 turbine requires further research, and is beyond the scope of the paper.

CRediT authorship contribution statement

Mark R. Fleming: Conceptualization, Methodology, Software, Formal analysis, Writing - original draft, Visualization. **Benjamin M. Adams:** Conceptualization, Methodology, Writing - review & editing, Visualization. **Thomas H. Kuehn:** Conceptualization, Writing - review & editing, Supervision, Project administration, Funding acquisition. **Jeffrey M. Bielicki:** Writing - review & editing, Project administration. **Martin O. Saar:** Conceptualization, Writing - review & editing, Supervision, Project administration, Funding acquisition.

Declaration of Competing Interest

The authors declare the following financial interests/personal relationships which may be considered as potential competing interests: Martin O. Saar declares a financial interest in the form of technology commercialization through CO2 POWER GmbH and TerraCOH Inc., of which he is a shareholder.

Acknowledgments

We gratefully acknowledge funding from the Initiative for Renewable Energy and the Environment (IREE), a signature program of the Institute on the Environment (IonE) at the University of Minnesota (UMN). We furthermore thank the Werner Siemens Foundation (Werner Siemens-Stiftung - WSS) for their support of the Geothermal Energy and Geofluids (GEG.ethz.ch) Group at ETH Zürich (ETHZ), Switzerland and ETHZ for its support of the GEG group. We also gratefully acknowledge funding from the Innovations at the Nexus of Food, Energy, and Water Systems (INFEWS) Grant (1739909), the Sustainability Institute, and the Center for Energy Research, Training, and Innovation (CERTAIN) at the Ohio State University (OSU). Finally, we thank the two reviewers for their thoughtful critique and feedback, which improved the manuscript. Any opinions, findings, conclusions, or recommendations in this material are those of the authors and do not necessarily reflect the views of the UMN, IREE, IonE, OSU, WSS, GEG, or ETHZ.

References

Adams, B.M., Kuehn, T.H., 2012. The Complementary Nature of CO2-Plume Geothermal (CPG) Energy Production and Electrical Power Demand Volume 6. pp. 1791. https://doi.org/10.1115/IMECE2012-88704. Energy, Parts A and B. ASME.

Adams, B.M., Kuehn, T.H., Bielicki, J.M., Randolph, J.B., Saar, M.O., 2015. A comparison of electric power output of CO2 Plume Geothermal (CPG) and brine geothermal systems for varying reservoir conditions. Applied Energy 140, 365–377. https://doi.org/10.1016/j.apenergy.2014.11.043.

Adams, B.M., Kuehn, T.H., Bielicki, J.M., Randolph, J.B., Saar, M.O., 2014. On the importance of the thermosiphon effect in CPG (CO2 plume geothermal) power systems. Energy 69, 409–418. https://doi.org/10.1016/j.energy.2014.03.032.

Ahmad, M., Casey, M., Sürken, N., 2009. Experimental assessment of droplet impact erosion resistance of steam turbine blade materials. Wear 267, 1605–1618. https://doi.org/10.1016/j.wear.2009.06.012.

Amann, F., Gischig, V., Evans, K., Doetsch, J., Jalali, R., Valley, B., Krietsch, H., Dutler, N., Villiger, L., Brixel, B., Klepikova, M., Kittilä, A., Madonna, C., Wiemer, S., Saar, M.O., Loew, S., Driesner, T., Maurer, H., Giardini, D., 2018. The seismo-hydromechanical behavior during deep geothermal reservoir stimulations: open questions tackled in a decameter-scale in situ stimulation experiment. Solid Earth 9, 115–137. https://doi.org/10.5194/se-9-115-2018.

Atrens, A.D., Gurgenci, H., Rudolph, V., 2010. Electricity generation using a carbon-dioxide thermosiphon. Geothermics 39, 161–169. https://doi.org/10.1016/j.geothermics.2010.03.001.

Atrens, A.D., Gurgenci, H., Rudolph, V., 2009. CO2 Thermosiphon for Competitive Geothermal Power Generation. Energy & Fuels 23, 553–557. https://doi.org/10.1021/ef800601z.

Bélteky, L., 1975. Problems related to operating thermal wells subject to scaling in Hungary. Geothermics 4, 57–65. https://doi.org/10.1016/0375-6505(75)90009-7.

Bielicki, J.M., Peters, C.A., Fitts, J.P., Wilson, E.J., 2015. An examination of geologic carbon sequestration policies in the context of leakage potential. International Journal of Greenhouse Gas Control 37, 61–75. https://doi.org/10.1016/j.ijggc.2015.02.023.

Bielicki, J.M., Pollak, M.F., Deng, H., Wilson, E.J., Fitts, J.P., Peters, C.A., 2016. The Leakage Risk Monetization Model for Geologic CO2 Storage. Environmental Science & Technology 50, 4923–4931. https://doi.org/10.1021/acs.est.5b05329.

Bielicki, J.M., Pollak, M.F., Fitts, J.P., Peters, C.A., Wilson, E.J., 2014. Causes and financial consequences of geologic CO2 storage reservoir leakage and interference with other subsurface resources. International Journal of Greenhouse Gas Control 20, 272–284. https://doi.org/10.1016/J.IJGGC.2013.10.024.

Boch, R., Leis, A., Haslinger, E., Goldbrunner, J.E., Mittermayr, F., Fröschl, H., Hippler, D., Dietzel, M., 2017. Scale-fragment formation impairing geothermal energy production: interacting H2S corrosion and CaCO3 crystal growth. Geothermal Energy 5, 4. https://doi.org/10.1186/s40517-017-0062-3.

Boch, R., Mindszenty, A., Szanyi, J., Deák, J., Leis, A., Kluge, T., Demény, A., Dietzel, M., 2016a. Growth dynamics of geothermal carbonate scales: Forensic studies based on high-resolution mineralogical & geochemical analyses. In: GeoTirol 2016 - Annual Meeting DGGV. Innsbruck, Austria.

Boch, R., Szanyi, J., Leis, A., Mindszenty, A., Deák, J., Kluge, T., Hippler, D., Demény, A., Dietzel, M., 2016b. Geothermal Carbonate Scaling: Forensic Studies Applying High-Resolution Geochemical Methods. In: Proceedings of the European Geothermal Congress. Strasbourg, France.

Brown, W.D., 2000. A Hot Dry Rock Geothermal Energy Concept Utilizing Supercritical CO2 Instead of Water. In: Proceedings of the Wenty-Fifth Workshop on Geothermal Reservoir Engineering. Palo Alto, California. pp. 1–6.

Buckley, S.E., Leverett, M.C., 1942. Mechanism of Fluid Displacement in Sands. Transactions of the AIME 146, 107–116. https://doi.org/10.2118/942107-G.

Chen, X., Gillespie, S.E., Oscarson, J.L., Izatt, R.M., 1992. Calorimetric determination of thermodynamic quantities for chemical reactions in the system CO2-NaOH-H2O from 225 to 325C. Journal of Solution Chemistry 21, 825–848. https://doi.org/10.1007/BF00651511.

Farshad, F.F., Garber, J.D., Rieke, H.H., Komaravelly, S.G., 2010. Predicting Corrosion in Pipelines, Oil Wells and Gas Wells; a Computer Modeling Approach. Scientia Iranica Transaction C: Chemistry and Chemical Engineering 17, 86–96.

Garapati, N., Randolph, J.B., Saar, M.O., 2015. Brine displacement by CO2, energy extraction rates, and lifespan of a CO2-limited CO2-Plume Geothermal (CPG) system with a horizontal production well. Geothermics 55, 182–194. https://doi.org/10.1016/j.geothermics.2015.02.005.

Garapati, N., Randolph, J.B., Valencia, J.L., Saar, M.O., 2014. CO2-Plume Geothermal (CPG) Heat Extraction in Multi-layered Geologic Reservoirs. Energy Procedia 63, 7631–7643. https://doi.org/10.1016/j.egypro.2014.11.797.

Gischig, V.S., Giardini, D., Amann, F., Hertrich, M., Krietsch, H., Loew, S., Maurer, H., Villiger, L., Wiemer, S., Bethmann, F., Brixel, B., Doetsch, J., Doonechaly, N.G., Driesner, T., Dutler, N., Evans, K.F., Jalali, M., Jordan, D., Kittilä, A., Ma, X., Meier, P., Nejati, M., Obermann, A., Plenkers, K., Saar, M.O., Shakas, A., Valley, B., 2019. Hydraulic stimulation and fluid circulation experiments in underground laboratories: Stepping up the scale towards engineered geothermal systems. Geomechanics for Energy and the Environment 100175. https://doi.org/10.1016/j.gete.2019.100175.

Haar, L., Gallagher, J.S., Kell, G.S., (U.S.), N.S.R.D.S, National Standard Reference Data System (U.S.), 1984. NBS/NRC steam tables : thermodynamic and transport properties and computer programs for vapor and liquid states of water in SI units. Hemisphere Pub. Corp., Washington [D.C.].

Hansen, E.W.M., Heitmann, H., Laksa, B., Loes, M., 1993. Numerical Simulation of Fluid Flow Behaviour Inside, and Redesign of a Field Separator. In: 6th International Conference on Multiphase Production. Cannes, France. pp. 117–129.

IPCC, 2014. Climate Change 2014: Mitigation of Climate Change. Contribution of Working Group III to the Fifth Assessment Report of the Intergovernmental Panel on Climate Change. Cambridge University Press, Cambridge. https://doi.org/10.1017/CBO9781107415416.

IPCC, 2005. IPCC Special Report on Carbon Dioxide Capture and Storage. Prepared by Working Group III of the Intergovernmental Panel on Climate Change. Cambridge University Press, Cambridge, United Kingdom.

Klein, S.A., Alvarado, F., 2002. Engineering Equation Solver. F-Chart Software.

Luhmann, A.J., Kong, X.-Z., Tutolo, B.M., Garapati, N., Bagley, B.C., Saar, M.O., Seyfried, W.E., 2014. Experimental dissolution of dolomite by CO2-charged brine at 100°C and 150bar: Evolution of porosity, permeability, and reactive surface area. Chemical Geology 380, 145–160. https://doi.org/10.1016/j.chemgeo.2014.05.001.

Matek, B., Gawell, K., 2015. The Benefits of Baseload Renewables: A Misunderstood Energy Technology. The Electricity Journal 28, 101–112. https://doi.org/10.1016/j.tej.2015.02.001.

Michael, K., Golab, A., Shulakova, V., Ennis-King, J., Allinson, G., Sharma, S., Aiken, T., 2010. Geological storage of CO2 in saline aquifers—A review of the experience from existing storage operations. International Journal of Greenhouse Gas Control 4, 659–667. https://doi.org/10.1016/j.ijggc.2009.12.011.

Moody, L.F., 1944. Friction factor for pipe flow. Transaction of the ASME 66, 671–684.

Pan, L., Oldenburg, C.M., Wu, Y.-S., Pruess, K., 2011. T2Well/ECO2N Version 1.0: Multiphase and Non-Isothermal Model for Coupled Wellbore-Reservoir Flow of Carbon Dioxide and Variable Salinity Water. Report LBNL-4291E. Berkeley National Laboratory, California.

Pan, L., Oldenburg, C.M., Wu, Y.-S., Pruess, K., 2009. Wellbore flow model for carbon dioxide and brine. Energy Procedia 1, 71–78. https://doi.org/10.1016/j.egypro.2009.01.012.

Piri, M., Prévost, J.H., Fuller, R., 2005. Carbon Dioxide Sequestration in Saline Aquifers: Evaporation, Precipitation and Compressibility Effects. Fourth Annual Conference on Carbon Capture and Sequestration DOE/NETL.

Pruess, K., 2008. On production behavior of enhanced geothermal systems with CO2 as working fluid. Energy Conversion and Management 49, 1446–1454. https://doi.org/10.1016/j.enconman.2007.12.029.

Pruess, K., 2006. Enhanced geothermal systems (EGS) using CO2 as working fluid—A novel approach for generating renewable energy with simultaneous sequestration of carbon. Geothermics 35, 351–367. https://doi.org/10.1016/j.geothermics.2006.08.002.

Pruess, K., 2005. ECO2N: A TOUGH2 Fluid Property Module for Mixtures of Water, NaCl, and CO2. Report LBNL-57952. Lawrence Berkeley National Laboratory, California.

Pruess, K., Oldenburg, C.M., Moridis, G., 1999. TOUGH2 User's Guide, Version 2. Report LBNL-43134. Lawrence Berkeley National Laboratory, California.

Randolph, J.B., Adams, B.M., Kuehn, T.H., Saar, M.O., 2012. Wellbore Heat Transfer in CO2-based Geothermal Systems. Geothermal Resources Council Transactions.

Randolph, J.B., Saar, M.O., 2011a. Coupling carbon dioxide sequestration with geothermal energy capture in naturally permeable, porous geologic formations: Implications for CO2 sequestration. Energy Procedia 4, 2206–2213. https://doi.org/10.1016/j.egypro.2011.02.108.

Randolph, J.B., Saar, M.O., 2011b. Combining geothermal energy capture with geologic carbon dioxide sequestration. Geophysical Research Letters 38. https://doi.org/10.1029/2011GL047265.

Randolph, J.B., Saar, M.O., 2011c. Impact of reservoir permeability on the choice of subsurface geothermal heat exchange fluid: CO2 versus water and native brine. Transactions - Geothermal Resources Council. pp. 521–526.

Saar, M.O., Randolph, J.B., Kuehn, T.H., 2012. Carbon Dioxide-Based Geothermal Energy Generation Systems and Methods Related Thereto. US Patent 8316955 B2.

Simmons, M.J.H., Wilson, J.A., Azzopardi, B.J., 2002. Interpretation of the Flow Characteristics of a Primary Oil–Water Separator from the Residence Time Distribution. Chemical Engineering Research and Design 80, 471–481. https://doi.org/10.1205/026387602320224058.

Span, R., Wagner, W., 1996. A New Equation of State for Carbon Dioxide Covering the Fluid Region from the Triple-Point Temperature to 1100 K at Pressures up to 800 MPa. Journal of Physical and Chemical Reference Data 25, 1509–1596. https://doi.org/10.1063/1.555991.

Spycher, N., Pruess, K., 2010. A Phase-Partitioning Model for CO2–Brine Mixtures at Elevated Temperatures and Pressures: Application to CO2-Enhanced Geothermal Systems. Transport in Porous Media 82, 173–196. https://doi.org/10.1007/s11242-009-9425-y.

Spycher, N., Pruess, K., 2005. CO2-H2O mixtures in the geological sequestration of CO2. II. Partitioning in chloride brines at 12–100°C and up to 600 bar. Geochimica et Cosmochimica Acta 69, 3309–3320. https://doi.org/10.1016/j.gca.2005.01.015.

Spycher, N., Pruess, K., Ennis-King, J., 2003. CO2-H2O mixtures in the geological sequestration of CO2. I. Assessment and calculation of mutual solubilities from 12 to 100°C and up to 600 bar. Geochimica et Cosmochimica Acta 67, 3015–3031. https://doi.org/10.1016/S0016-7037(03)00273-4.

Tutolo, B.M., Kong, X.-Z., Seyfried, W.E., Saar, M.O., 2015. High performance reactive transport simulations examining the effects of thermal, hydraulic, and chemical (THC) gradients on fluid injectivity at carbonate CCUS reservoir scales. International Journal of Greenhouse Gas Control 39, 285–301. https://doi.org/10.1016/j.ijggc.2015.05.026.

Tutolo, B.M., Luhmann, A.J., Kong, X.-Z., Saar, M.O., Seyfried, W.E., 2014. Experimental Observation of Permeability Changes In Dolomite at CO2 Sequestration Conditions. Environmental Science & Technology 48. https://doi.org/10.1021/es4036946.

Walsh, S.D.C., Garapati, N., Leal, A.M.M., Saar, M.O., 2017. Calculating thermophysical fluid properties during geothermal energy production with NESS and Reaktoro. Geothermics 70, 146–154. https://doi.org/10.1016/j.geothermics.2017.06.008.